Giant resonances in the ^{26}Mg$(e,e'\alpha_0)^{22}$Ne reaction

L. A. A. Terremoto,* V. P. Likhachev, M. N. Martins, H. J. Emrich,† G. Fricke,† Th. Kröhl,† and K. W. Neff†
Laboratório do Acelerador Linear, Instituto de Física da Universidade de São Paulo,
Caixa Postal 66318, 05315-970 São Paulo, SP, Brazil
(Received 14 April 1997)

The fivefold differential cross section of the reaction ^{26}Mg$(e,e'c)$ was measured for transferred momenta of 0.35 and 0.54 fm^{-1} and emitted particle angles from $-10°$ to 270° with respect to the transferred-momentum direction. Angular correlation functions for the emitted α_0 were obtained from the data. A model-independent analysis allowed us to obtain the $E0$, $E1$, and $E2$ multipole components of the ^{26}Mg$(e,e'\alpha_0)^{22}$Ne cross section, between 14 and 26 MeV of excitation energy. The $E1$ component shows a bump around 16.5 MeV, associated with the $T_<$ isospin component of the giant dipole resonance. The evaluated strengths associated with the α_0 decay channel, presented in percentage of the respective energy-weighted sum rules are 0.45(7)% for $E1$, 1.4(3)% for $E2$, and 0.2(1)% for $E0$.
[S0556-2813(97)05111-X]

PACS number(s): 24.30.Cz, 25.30.Fj, 23.60.+e, 27.30.+t

I. INTRODUCTION

Electrodisintegration experiments in coincidence, $(e,e'c)$, accomplished at high duty factor electron accelerators [1–4] and storage rings [5], demonstrated the possibility to separate and study, in some cases model independently, several reaction mechanisms—direct, resonant, preequilibrium, and statistical—providing information about important and complex aspects of nuclear dynamics. In particular, $(e,e'\alpha_0)$ experiments in the giant resonance region on spin-0 nuclei are especially interesting since the small contribution of the direct process and the small number of amplitudes involved simplify the analysis and allow a model-independent multipole decomposition of the resonance cross section.

This work is concerned with a study of the excitation and decay of giant resonances in the ^{26}Mg$(e,e'\alpha_0)^{22}$Ne reaction and, in particular, with a model-independent study of the isoscalar electric quadrupole resonance (GQR). This resonance has been intensively studied in many nuclei, by means of various reactions: (e,e') [6,7], (p,γ) [8], (α,γ_0) [9], $(\alpha,\alpha'\alpha)$ [10], and (α,α') [11,12].

II. EXPERIMENTAL PROCEDURE

Using the electron beam from the MAMI-A2 [13] microtron, a 1.1-mg/cm^2 enriched ^{26}Mg target [99.70(5)% ^{26}Mg, 0.21(3)% ^{24}Mg, and 0.09(3)% ^{25}Mg] was bombarded at 183.5 MeV with typical cw currents of 10–12 μA. The target thickness ensures small energy losses in the target material for α particles with energies above 2 MeV.

Scattered electrons were detected in the focal plane of a 180° double-focusing magnetic spectrometer [14] (solid angle $\Delta\Omega = 4$ msr) by a 300-channel detection system ($\Delta P/P = 0.0216\%$ per channel) [15] at scattering angles of 22° and 35°, to define the transferred momenta q of 0.35 and 0.54 fm^{-1}, respectively. The relative detection efficiency of each channel was determined [15] measuring the elastic scattering of electrons on ^{12}C and moving the detector ladder along the focal plane, so that the same part of the spectrum was measured by each detector channel.

Decay charged particles were detected in an array of ten silicon surface barrier detector telescopes arranged in a plane rotated about the q axis by $\phi = 225°$ (for $q = 0.35$ fm^{-1}) or $\phi = 240°$ (for $q = 0.54$ fm^{-1}) from the electron-scattering plane. The array of telescopes, developed at the Max Planck Institute for Nuclear Physics in Heidelberg (see Fig. 1), allowed measurements of the decay correlation angle θ_c in that plane, from $-10°$ (forward of q) to 180° (opposite to q) and beyond, up to $\theta_c = 270°$. The out-of-scattering-plane geometry is very useful since it allows the measurement of the angular correlation without a gap corresponding to the angular region blocked in the scattering plane by the incoming beam.

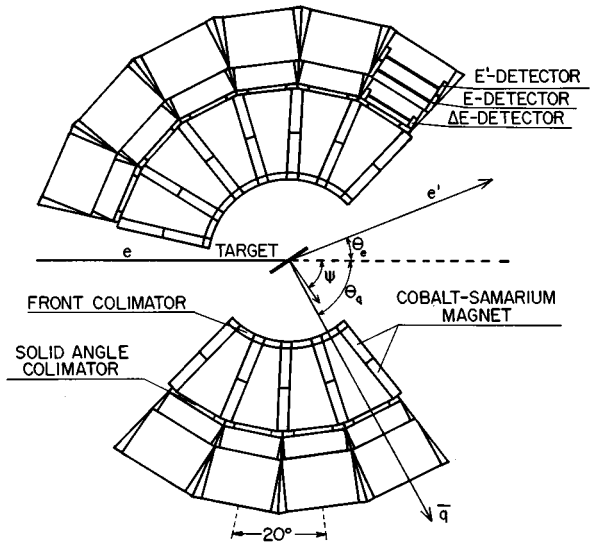

FIG. 1. Charged particle detector arrangement.

*Presently at IPEN/CNEN-SP, São Paulo, SP, Brazil.

†Formerly at Institut für Kernphysik der Johannes Gutenberg Universität, D-55099 Mainz, Germany.

TABLE I. Summary of the performed measurements: θ_e is the electron-scattering angle, q is the momentum transferred, θ_q is the momentum-transfer angle (see Fig. 1), ϕ_c and θ_c are the azimuthal and polar angles of the emitted particle, and ψ is the angle between the normal to the target surface and the incoming beam direction.

θ_e	q (fm^{-1})	θ_q	ϕ_c	ψ	θ_c
				$-55°$	0°,20°,40°,160°,180°,200°,220°
					10°,30°,50°,170°,190°,210°,230°
22°	0.35	62.2°	225°	18°	50°,70°,90°,110°,130°,150°,230°
					60°,80°,100°,120°,140°,160°,240°
				$-60°$	0°,20°,40°,60°,140°,160°,180°,200°,220°,240°
35°	0.54	62°	240°		$-10°$,10°,30°,50°,130°,150°,170°,190°,210°,230°
				38°	40°,60°,80°,100°,120°,140°,220°,240°,260°,280°
					30°,50°,70°,90°,110°,130°,210°,230°,250°,270°

Each telescope contains three silicon surface barrier detectors. The ΔE detectors are 72 μm thick (on the average) and the E and E' detectors are 1012 μm thick (also on the average). Each telescope was installed in a holder, together with a collimator and a cobalt-samarium magnet. The collimator defines the solid angle seen by the telescope, while the permanent magnet, placed before the collimator, reduces the background caused by low energy electrons emitted from the target. To reduce dark current, the detectors were cooled using methyl alcohol at -20 °C. The distance between target and frontal collimator was 36.5 mm, and the telescope solid angle was $\Delta\Omega_c = 39.76$ msr with a half-angle aperture of $\Delta\theta_c = \pm 6.58°$. The telescopes were arranged around the target in steps of 20°. The central holder of the scattering chamber can be rotated around the q axis with respect to the scattering plane.

The data acquisition was done in an event-by-event mode. The signals from the charged particle detectors were amplified by charge sensitive preamplifiers. The T signals from the preamplifiers were used for time coincidence, while the E signals were used for recording the energy deposited in the detector. For each coincidence event the following data were recorded for off-line analysis: (1) electron channel number, (2) telescope number, (3) telescope detector number, (4) energy deposited in the charged particle detectors, and (5) time difference between charged particle and electron signals. Table I shows the array of kinematical variables where data were taken.

III. DATA REDUCTION

The experimental data obtained contain information about several reactions, but this article is concerned only with the ^{26}Mg$(e,e'\alpha_0)^{22}$Ne reaction channel, and only the aspects relevant to this subject will be described.

The classification of events was divided in many steps in order to obtain the angular correlation for the α_0 reaction channel. The steps will be described below.

A. Particle-type identification

In order to decrease as much as possible the detection threshold for α particles, the pulse-shape-discrimination method was used [16], and information about the particle energy and its type was obtained from coincidence spectra between signals from the electron counters and the first (ΔE) telescope detector. This method is based on a property of silicon surface barrier detectors: The rise time of the pulse depends on the particle type and its kinetic energy. So the information about the particle type and its energy is contained in the two-dimensional time-to-digital converter (TDC) and analog-to-digital converter (ADC) spectrum. This 256×256 matrix of the time difference between the electron counter signal and the signal from the ΔE detector (TDC register) and the particle energy deposited in the ΔE detector (ADC register) is shown in Fig. 2. Two groups (or bands) of events can be seen. The lower band corresponds to p, d, and t particles, and the upper band to ^{3}He and ^{4}He particles. These two bands appear due to the different charge collection time (plasma effect) for low (p,d,t) and high (^{3,4}He) ionizing particles.

The extraction of events corresponding to ^{3,4}He was performed by drawing a two-dimensional gate around this particle group, observed in the energy-time matrix. The separation of ^{4}He and ^{3}He contributions was done based on the difference in their separation energies (S_c), in a later stage of the process. Random coincidence events are uniformly dis-

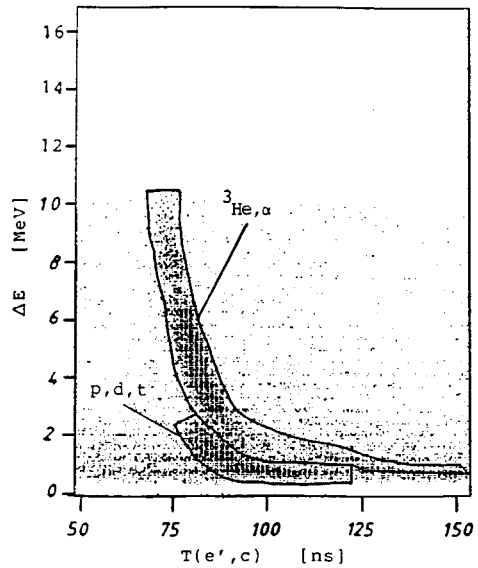

FIG. 2. Energy-time matrix from the ^{26}Mg$(e,e'c)$ experimental data for $\theta_e = 35°$ and $\theta_c = 60°$.

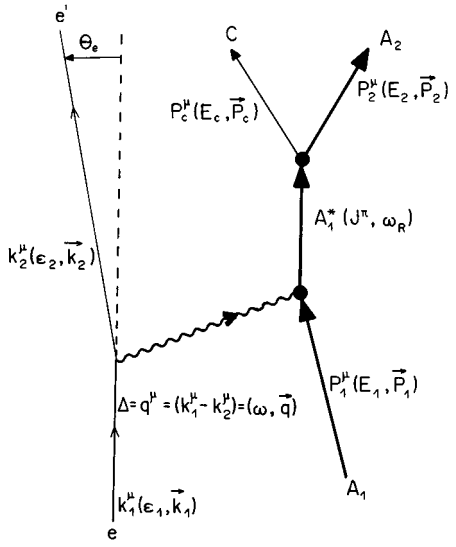

FIG. 3. Diagram of the coincidence reaction $A_1(e,e'c)A_2$ in first Born and resonance approximations.

tributed along the energy-time matrix. The contribution of the random coincidence background was determined by shifting the two-dimensional gate out of the bands.

To improve the pulse shape discrimination, all ΔE detectors were mounted with the back electrode facing the target [16].

B. Separation of decay modes

In order to identify and separate decays to different final states of product nuclei, the coincidence events were organized in two-dimensional energy-energy matrices of order 300×256 (300 is the number of electron detectors in the focal plane). Each matrix element corresponds to a correlated pair of energy of scattered electron and kinetic energy of the decay particle (E_c).

The energy balance of a two-particle disintegration reaction can be written as

$$\varepsilon_1-\varepsilon_2=\omega=E_c+E_2+S_c\,, \tag{1}$$

where S_c is the separation energy. The notation is explained in Fig. 3. Since E_2 is usually small, the dependences of ω versus E_c, for different final states, appear as parallel straight lines in a plot of $\omega\times E_c$ (Dalitz diagram). The events corresponding to different final states are located on different straight bands, as illustrated by the typical Dalitz diagram shown in Fig. 4.

The profile of the Dalitz diagram for a fixed ω represents the excitation energy spectrum of the daughter nucleus, as shown in Fig. 5 for $\omega=20.1$ MeV. The energy resolution achieved in the experiment allows a reliable separation of α_0 and α_1 peaks.

The extraction of events of a given decay channel was performed by drawing a two-dimensional gate around the band which corresponded to the respective kinematics line. Background from other reactions was subtracted by shifting the gate out of the band.

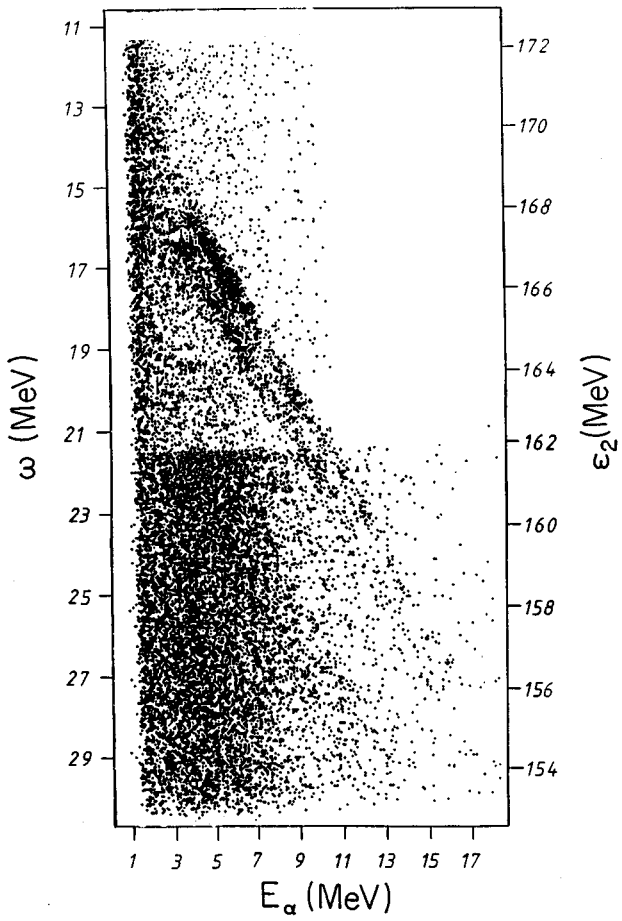

FIG. 4. Dalitz diagram from the ^{26}Mg$(e,e'\alpha)$ experimental data for $\theta_e=22°$ and $\theta_\alpha=0°$. The figure is obtained merging data from two runs with different settings of the electron spectrometer. That causes the change in the background.

C. Absolute normalization

The absolute normalization factor for the coincidence spectra was obtained by normalizing the theoretical value of the elastic ^{26}Mg(e,e') cross section, reduced by a radiation factor, to the experimental value, measured at the same experimental conditions as the ^{26}Mg$(e,e'c)$ cross section. The

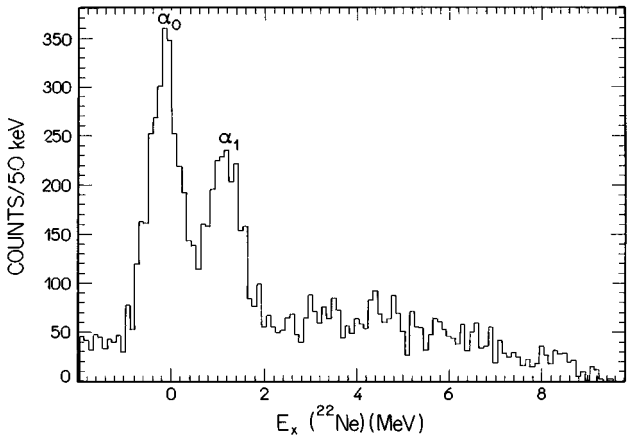

FIG. 5. Excitation energy spectrum of the daughter nucleus ^{22}Ne for $\theta_e=35°$ and $\theta_\alpha=20°$ and $\omega=20.1$ MeV.

theoretical value of the elastic scattering cross section was calculated by means of the phase-shift code HADES [17], using for the ground-state charge-density distribution a two-parameter Fermi function:

$$\rho(r)=\rho_0\{1+\exp[(r-c)/z)]\}^{-1}, \tag{2}$$

with parameters $c=3.06(5)$ fm and $z=0.524(32)$ fm, from Ref. [18].

The theoretical value was reduced by the factor $\exp(-\delta_s)$, which takes into account the Schwinger radiation correction and thus makes the theoretical and experimental results consistent. The correction for elastic scattering was calculated using the ultrarelativistic approximation expression ($\varepsilon_1 \gg m_e$, $q^2 \gg m_e$) [19]:

$$\delta_s=\left(\frac{2\alpha}{\pi}\right)\left\{\left[\ln\left(\frac{\varepsilon_1}{\Delta E}\right)-\left(\frac{13}{12}\right)\right]\left[\ln\left(\frac{q^2}{m_e^2}\right)-1\right] + \frac{17}{36}+\frac{1}{2}\left[\frac{\pi^2}{6}-L_2\left(\cos^2\frac{\theta_e}{2}\right)\right]\right\}, \tag{3}$$

where $\Delta E=0.6$ MeV is the cutoff energy, m_e is the rest mass of the electron, and $L_2(x)$ is the Spence function [19]: $L_2(x)=-\int_0^x\{[\ln(1-y)]/y\}dy$. The inelastic cross sections were corrected by the Schwinger radiation factor according to [19,20].

As a result of the data reduction procedure, $(e,e'\alpha_0)$ spectra were obtained, corrected for random coincidences, and absolutely normalized, for each telescope angle. These angles and the corresponding detector solid angles were transformed from the laboratory system to the center-of-momentum (c.m.) system, which has the z axis oriented along the momentum transferred (see next item). Since the direction of momentum transfer depends on the excitation energy, an average direction for the range under study was chosen and the new, so-called correlation angles are read with respect to this direction. Angular correlations (cross section as a function of correlation angles) were obtained for each interval of the excitation energy, in steps of 0.2 MeV. As an example, Fig. 6 shows angular correlations for two energy bins, taken at the two momentum transfers $q=0.35$ and 0.54 fm^{-1}.

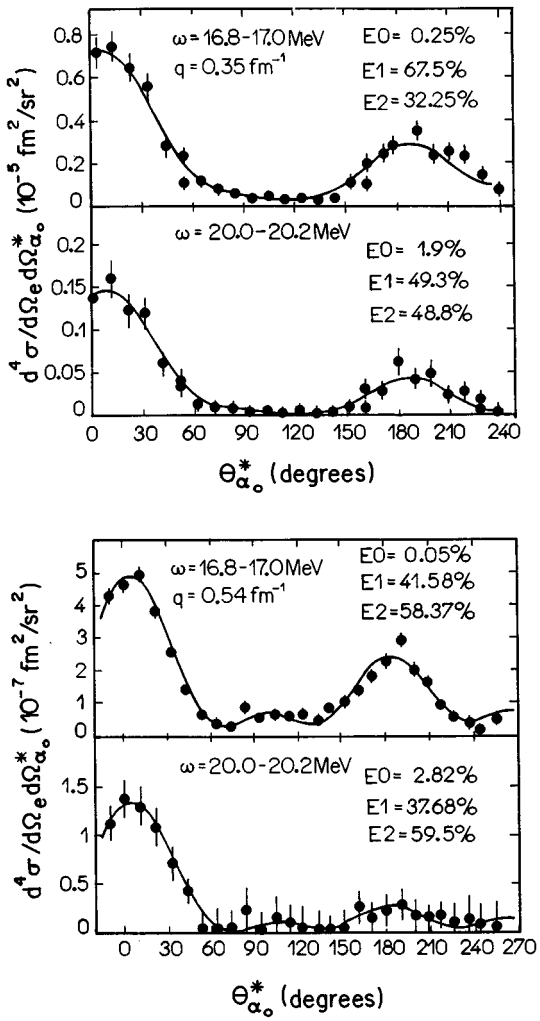

FIG. 6. Angular correlation function for the reaction ^{26}Mg$(e,e'\alpha_0)^{22}$Ne. The curves are the results of fitting with a series of Legendre polynomials [see Eq. (6)].

IV. DATA ANALYSIS

Figure 7 shows schematically the process of excitation, in the giant resonance energy region of ^{26}Mg, with subsequent decay to final states in ^{25}Na and ^{22}Ne nuclei. Table II shows characteristics of the transitions involved in the excitation of $E0$, $E1$, and $E2$ giant resonances in ^{26}Mg, with subsequent α_0 and α_1 decays.

In the one-photon-exchange approximation, the fivefold differential cross section of an $(e,e'c)$ reaction, in the c.m. frame, can be written as [21]

$$\frac{d^5\sigma}{d\varepsilon_2 d\Omega_e d\Omega_c^*}=\frac{2\alpha^2}{q^4}\frac{k_2}{k_1}\left(\frac{\xi^* w}{\pi M_1}\right)\left\{V_C\left(\frac{w}{M_1}\right)^2\left|J^0\right|^2 + V_T(|J^{+1}|^2+|J^{-1}|^2) + V_{CT}\left(\frac{w}{M_1}\right)\sqrt{2}\ \mathrm{Im}(J^0)^*(J^{+1}+J^{-1}) + V_{TT}2\ \mathrm{Re}(J^{+1})^*J^{-1}\right\}, \tag{4}$$

where $V_{C,T,CT,TT}$ are the kinematical factors of electron scattering variables in the laboratory frame and $J^{0,+1,-1}$ are the helicity components of the transition matrix elements of the nuclear current operator (J^0 is the longitudinal component, and $J^{+1,-1}$ are the transverse components) expressed in the c.m. frame. Figure 3 illustrates the notation used. ξ^* means that the value ξ is related to the c.m. frame.

The advantage of coincidence experiments, when compared to singles inelastic measurements, can be seen from Eq. (4). The coincidence cross section contains additional interference terms, which allows the study of small ampli-

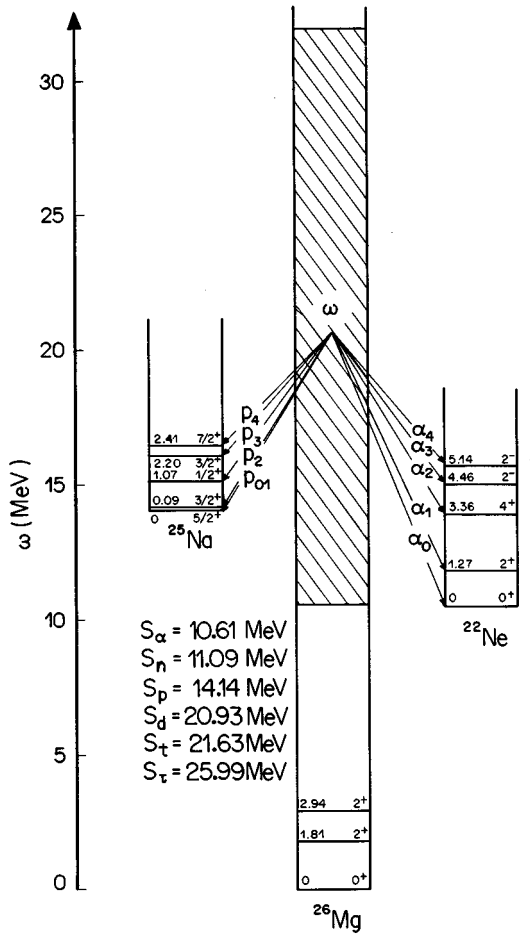

FIG. 7. Energy level diagrams of the target (^{26}Mg) and daughter (^{22}Ne and ^{25}Na) nuclei. The particle separation energies for ^{26}Mg are shown in the lower left.

TABLE II. Characteristics of the giant resonances in the ^{26}Mg$(e,e'\alpha)^{22}$Ne reaction: J^π is the spin and parity of the ^{26}Mg excited state, $S^\pi_{A_2}$ is the spin and parity of the ^{22}Ne final state, L is the relative orbital angular momentum of the emitted particle, and J_c is the total angular momentum of the emitted particle.

^{26}Mg			^{22}Ne			
GR	J^π	Decay	$S^\pi_{A_2}$	L	J_c	Partial waves
$E0$	0^+	α_0	0^+	0	0	s
$E1$	1^-	α_0	0^+	1	1	p
$E2$	2^+	α_0	0^+	2	2	d

tudes through their interference with big ones and also to determine the relative phases of matrix elements. There is also the possibility of determining spins and parities of resonances, in a model-independent way, via the analysis of the angular distributions of emitted particles, as in the case of real photons.

Four combinations of transition matrix elements in Eq. (4) can be kinematically separated using the explicit dependence on the emitted particle variables, which allows, in some cases, to separate the contributions of different mechanisms in a model-independent way.

In resonance approximation (see Fig. 3) the matrix elements in Eq. (4) can be derived in the form of a multipole expansion and can be factored into nuclear excitation and decay amplitudes [21]. A further simplification occurs for spin-0 systems. Finally, in the extreme relativistic limit (ERL) for initial and final electrons and assuming the static limit of the resonance approximation, the differential cross section for electric transitions of multipolarity L and for spin and parity of target and residual nuclei and emitted particle $J^\pi=0^+$ [as occurs in the ^{26}Mg$(e,e'\alpha_0)^{22}$Ne reaction] can be written [21] as

$$\frac{d^5\sigma}{d\varepsilon_2 d\Omega_e d\Omega_{\alpha_0}} = \sigma_M (2L+1) A_0(L) |CL|^2 \left[P_L(\cos\theta^*_{\alpha_0})^2 + \left(\frac{1}{2}+\tan^2\frac{\theta_e}{2}\right)\frac{|TL|^2}{|CL|^2}\frac{1}{L(L+1)} P^1_L(\cos\theta^*_{\alpha_0})^2 \right.$$
$$-\left(\frac{1}{2}+\tan^2\frac{\theta_e}{2}\right)\frac{|TL|}{|CL|}\frac{2}{\sqrt{L(L+1)}} P_L(\cos\theta^*_{\alpha_0}) P^1_L(\cos\theta^*_{\alpha_0}) \sin\phi^*_{\alpha_0} - \frac{1}{2}\frac{|TL|^2}{|CL|^2}$$
$$\left. \times \frac{1}{L(L+1)} P^1_L(\cos\theta^*_{\alpha_0})^2 \cos 2\phi^*_{\alpha_0} \right], \tag{5}$$

where

$$\sigma_M = \left(\frac{\alpha Z}{2\varepsilon_1}\right)^2 \frac{\cos^2(\theta_e/2)}{\sin^4(\theta_e/2)}$$

is the Mott cross section, Z is the charge of the target nucleus, CL and TL are the longitudinal and transverse electric form factors, respectively, which describe the excitation of multipolarity L, $A_0(L)$ are the decay coefficients, and $\theta^*_{\alpha_0}$ and $\phi^*_{\alpha_0}$ are the polar and azimuthal angles of the emitted α particle, referred to the direction of the momentum transfer.

For our kinematical conditions, it is possible to neglect the contribution of the transverse form factors, when compared to the longitudinal ones. Figure 8 shows a comparison among the terms between brackets in Eq. (5) for $E2$ transitions, calculated for $\theta_e=35°$ and $\theta_{\alpha_0}=240°$. The ratio of transverse to longitudinal form factors was calculated using Siegert's theorem [22] and assuming an average excitation

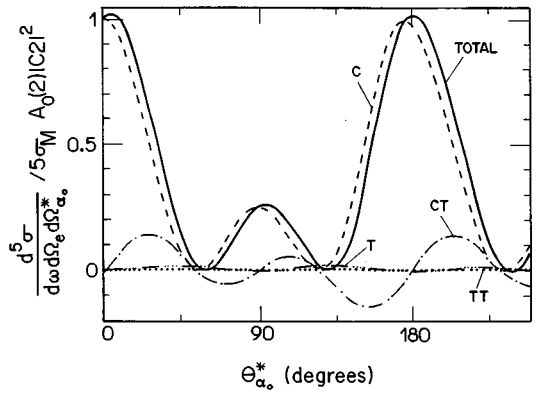

FIG. 8. Contributions of different terms in the differential cross section of $E2$ transitions for $\theta_e = 35°$ and $\phi_c = 240°$.

energy of 20 MeV. The total cross section coincides with the longitudinal one within 5%. The same situation holds for $L = 1$.

Thus, with a little loss of accuracy, but a great gain in simplicity in the analysis, the differential cross section for a set of multipoles up to 2 can be written as

$$\frac{d^5\sigma}{d\varepsilon_2 d\Omega_e d\Omega_{\alpha_0}} = \sigma_M \left| \sum_{L=0}^{2} \sqrt{(2L+1)A_0(L)}\, CL\, e^{i\delta_L} P_L(\cos\theta^*_{\alpha_0}) \right|^2, \quad (6)$$

where δ_L is the phase of the product of CL and $A_0(L)$. The sum on L in Eq. (6) is limited to 2, since higher multipoles, in our region of q, have negligible contribution.

We evaluated the $E3$ contribution to the total cross section using a distorted wave Born approximation (DWBA) code [17] and assuming a transition charge density given by the modified Tassie model [23]. The transition strength was expressed as fraction of the electromagnetic sum rule [24–26]. Considering the isoscalar $E3$ exhausting 100% of its energy-weighted sum rule (EWSR), it would have a contribution to the total cross section of 1% at $q = 0.35$ fm^{-1} and 2.5% at $q = 0.54$ fm^{-1}.

For each energy bin, the coefficients of the Legendre polynomials in Eq. (6) were fitted to get the experimental value of the cross section, obtaining as a result the products $A_0(L)|CL|^2$ for $L = 0,1,2$. Using the results for $A_0(L)|CL|^2$, the cross section for each multipolarity was obtained as

$$\frac{d^3\sigma_L}{d\varepsilon_2 d\Omega_e} = \sigma_M (2L+1) A_0(L) |CL|^2 \int [P_L(\cos\theta^*_{\alpha_0})]^2 d\Omega_{\alpha_0}. \quad (7)$$

In this method, however, when more than two resonances are present, there is an intrinsic ambiguity and only the highest multipole ($E2$) is determined unambiguously [27]. For $A_0(0)|C0|^2$ and $A_0(1)|C1|^2$, we have two different sets of solutions: One presents a high monopole strength with a small dipole and the other the inverse situation, a small monopole and a higher dipole. These two sets are shown in Figs. 9 and 10. The choice between the two sets was made

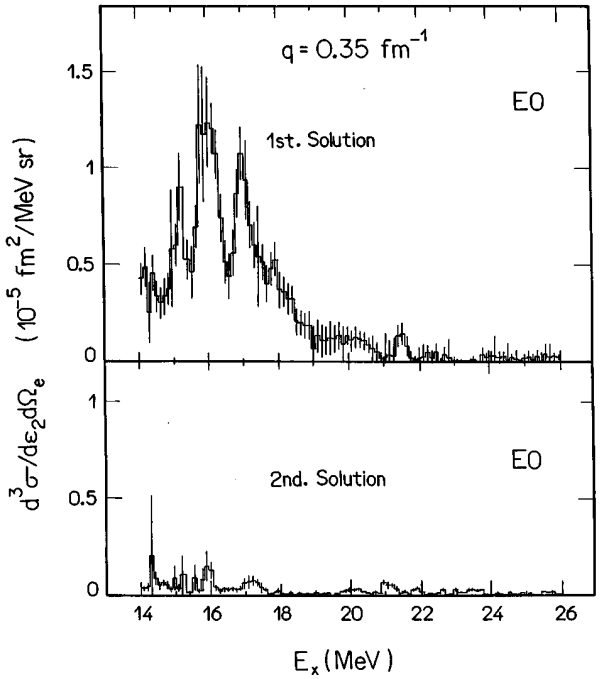

FIG. 9. Solutions for the $E0$ component of the ^{26}Mg$(e,e'\alpha_0)^{22}$Ne cross section at $q = 0.35$ fm^{-1}.

by comparing the shape of the obtained $E1$ cross section with the shape of the $E1$ cross section extracted from the inverse reaction ^{22}Ne$(\alpha,\gamma_0)^{26}$Mg [9], which clearly favored the second set (see Fig. 10).

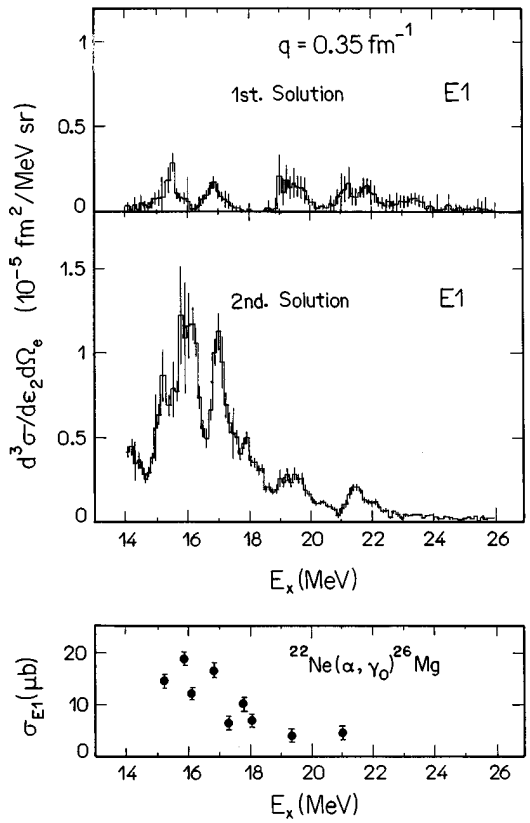

FIG. 10. Solutions for the $E1$ component of the ^{26}Mg$(e,e'\alpha_0)^{22}$Ne cross section at $q = 0.35$ fm^{-1} (this work) and ^{22}Ne$(\alpha,\gamma_0)^{26}$Mg [9].

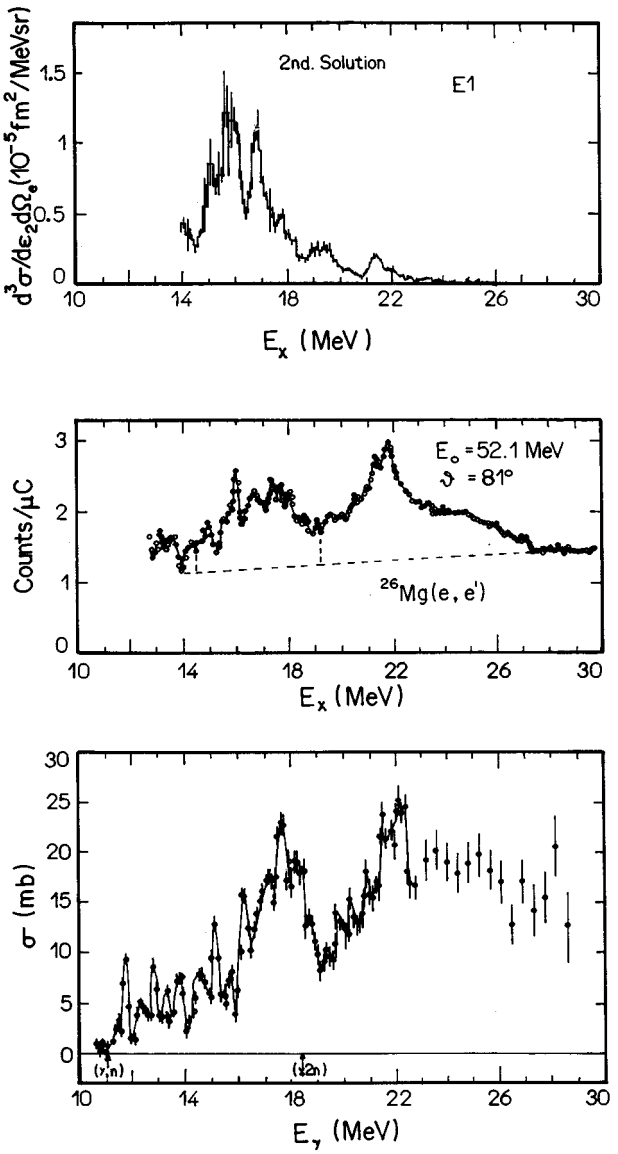

FIG. 11. $E1$ component of the cross section, obtained from the following reactions: ^{26}Mg$(e,e'\alpha_0)^{22}$Ne (upper part, this work), ^{26}Mg(e,e') (middle part [28]), and ^{26}Mg(γ,n) (lower part [30]).

V. RESULTS AND DISCUSSION

Figure 11 shows the final results of the model-independent extraction of the $E1$ cross section for the reaction ^{26}Mg$(e,e'\alpha_0)^{22}$Ne in comparison with $E1$ cross sections for ^{26}Mg(e,e') [28,29] and ^{26}Mg(γ,n) [30] reactions. Since the ground state of ^{26}Mg has isospin $T=1$, the giant dipole resonance (GDR, $\Delta T=1$) should be split into two components: $T_<=1$ and $T_>=2$, separated by about 4.6 MeV in excitation energy, according to the evaluation in Ref. [31]. In (e,e') and (γ,n) spectra, two bumps are noticed: One is located at 14–19 MeV, the other at 20–28 MeV. These bumps were interpreted [28–30] as two isospin components of the GDR. The observed energy of the splitting and the ratio of the cross sections at the maximum of the bumps are larger than evaluated in [31]. In the $(e,e'\alpha_0)$ spectra, just one bump, split in two peaks, is observed. The energy position of this bump coincides with the left bump present in the (e,e') and (γ,n) spectra. The right bump is absent in $(e,e'\alpha_0)$ spectra. Since only the $T_<$ component has an isospin-allowed α_0-decay mode, the absence of the right bump in the $(e,e'\alpha_0)$ spectra supports the argument that the splitting of the GDR observed in (e,e') and (γ,n) spectra is connected with isospin.

The $T_<$ component of the GDR, observed in $(e,e'\alpha_0)$ spectra, shows some structure (two peaks) which is also present in the results of Refs. [28–30].

The strength of the $E1$ resonance in the reaction ^{26}Mg$(e,e'\alpha_0)^{22}$Ne was analyzed in terms of the electromagnetic sum rule. These classical sum rules do not account for interference between isoscalar and isovector excitations, and are used in this work only as a convenient scale to measure the resonance strength. Such an approach allows one to compare results obtained in different kinematical conditions and even in different reactions [32], since sum rules are absolute units, depending only on the ground-state charge distribution.

The energy-weighted sum rules were calculated using the expressions from Refs. [24–26]:

$$S(E0)=\sum_{\omega_R} B_{C0}(E_x)E_x=\frac{2\hbar^2 Q}{m_p}\langle r^2\rangle,$$

$$S(E1,\Delta T=1)=\sum_{\omega_R} B_{C1}(E_x)E_x=\frac{9\hbar^2}{8\pi m_p}\frac{NZ}{A},$$

$$S(EL,L>1)=\sum_{\omega_R} B_{CL}(E_x)E_x=\frac{L(2L+1)^2\hbar^2 Q}{8\pi m_p}\langle r^{2L-2}\rangle, \tag{8}$$

where E_x is the excitation energy, m_p is the mass of the proton, $Q=Z^2/A$ for isoscalar excitations and $Q=NZ/A$ for isovector ones, and $\langle r^{2L-2}\rangle$ is the $(2L-2)$ moment of the ground-state charge distribution of the nucleus: $\langle r^{2L-2}\rangle=\int\rho(\vec{r})r^{2L-2}d\vec{r}$. Using $\langle r^2\rangle^{1/2}=3.06(5)$ fm, which was obtained by numerical integration of the ground-state charge distribution [see Eq. (2)], then

$$S(E0,\Delta T=0)=4304\ \text{MeV fm}^4,$$

$$S(E1,\Delta T=1)=96\ \text{MeV fm}^2,$$

$$S(E2,\Delta T=0)=4282\ \text{MeV fm}^4. \tag{9}$$

The resonance strength, in the excitation energy range 14–26 MeV, was evaluated using the first Born expression for the cross section for a spinless nucleus in the relativistic limit $(m_e\rightarrow 0)$ [33,34] and a model-independent expansion of the reduced transition probability [35,36]. For $L\geqslant 1$,

$$\frac{d\sigma_{CL}}{d\Omega}=4\pi\sigma_M^1\left(\frac{\Delta^2}{q^2}\right)^2 f_{rec}B_{CL}(q)q^{2L}[(2L+1)!!]^{-2}, \tag{10}$$

and for $L=0$,

$$\frac{d\sigma_{C0}}{d\Omega}=4\pi\sigma_M^1\left(\frac{\Delta^2}{q^2}\right)^2 f_{rec}B_{C0}(q)q^4[15]^{-2}, \tag{11}$$

where

TABLE III. $E0$, $E1$, and $E2$ transition strengths observed in ^{26}Mg.

Multipolarity	Reaction	Energy range (MeV)	R (% EWSR)
	^{26}Mg$(e,e'\alpha_0)^{22}$Ne (this work)	14.0–26.0	0.45(7)
$E1$	^{22}Ne$(\alpha,\gamma_0)^{26}$Mg [9]	14.8–21.0	0.7
	^{26}Mg(γ,n) [30]	11.0–28.0	58
	^{26}Mg(e,e) [28,29]	14.5–28.0	48
$E2$	^{26}Mg$(e,e'\alpha_0)^{22}$Ne (this work)	14.0–26.0	1.4(3)
	^{22}Ne$(\alpha,\gamma_0)^{26}$Mg [9]	15.0–21.4	6(2)
$E0$	^{26}Mg$(e,e'\alpha_0)^{22}$Ne (this work)	14.0–26.0	0.2(1)

$$\left(\frac{B_{CL,L\geq 1}(q)}{B_{CL}(q=0)}\right)^{1/2}=1-\frac{q^2\langle r_{CL}^2\rangle_{\rm tr}}{2(2L+3)}+\frac{q^4\langle r_{CL}^4\rangle_{\rm tr}}{8(2L+3)(2L+5)}-\cdots, \tag{12}$$

$$\left(\frac{B_{C0}(q)}{B_{C0}(q=0)}\right)^{1/2}=1-\frac{q^2\langle r_{C0}^2\rangle_{\rm tr}}{20}+\frac{q^4\langle r_{C0}^4\rangle_{\rm tr}}{840}-\cdots, \tag{13}$$

$$\langle r_{CL}^l\rangle_{\rm tr}=\int r^{L+l+2}\rho_L(r)dr \Big/ \int r^{L+2}\rho_L(r)dr, \tag{14}$$

$$\langle r_{C0}^l\rangle_{\rm tr}=\int r^{l+4}\rho_0(r)dr \Big/ \int r^4\rho_0(r)dr, \tag{15}$$

$\rho_L(r)$ is the transition charge distribution, σ_M^1 is the Mott cross section for $Z=1$ [see Eq. (5)], Δ^2 is the four-momentum transfer squared ($\Delta^2=q^2-\omega^2$, neglecting recoil), and

$$f_{\rm rec}\cong\left[1+\frac{2k_1}{M}\sin^2\frac{\theta_e}{2}\right]^{-1}.$$

The resonance strength can be written as a fraction of the EWSR as

$$R=\frac{B_{CL}(E_x)E_x}{\mathrm{EWSR}(EL,\Delta T)}\times 100.$$

Since only two different q's were measured, the values of $\langle r^l\rangle$, needed for the extrapolation, were calculated using a model for the transition charge distribution, with fixed parameters. In order to estimate the model dependence of the extrapolation results, several models were used [23,37–40], which express the transition charge-density distribution as a function of the ground-state charge-density distribution. We used for the ground-state distribution, following [41], a two-parameter Fermi function with parameters $c=(0.9–1.2)c_0$ (extreme cases) and $t=t_0$, where c_0 and t_0 are the parameters obtained for the ground state distribution by Ref. [18].

The range of $\langle r^l\rangle_{\rm tr}^{1/l}$ was 2.7–4.2 fm. That leads to uncertainties for the extracted resonance strength of $\pm 4.5\%$. This uncertainty due to different transition radii was included in the total uncertainty of the resonance strength. The results presented for the resonance strength are therefore model independent within the error bars.

Coulomb correction of the electron wave functions was accounted for by using $q'=q(1+1.8Z/A^{1/3}k_1)$ [42]. This procedure was assessed by comparing the result with a more accurate calculation, performed in the DWBA [17] for one of the models [Goldhaber-Teller (GT) model]. The results were very close.

In the evaluation of the resonance strength, the resonance energy for the $E1$ and $E2$ resonances was chosen as the energy position of the resonance structure in the spectrum (17 MeV). For the $E0$ resonance, the average energy of the measurement interval (20 MeV) was chosen, since no resonance structure could be identified in the spectrum.

The result for the $E1$ strength is shown in Table III, in percentage of the respective EWSR [Eq. (8)]. The $E1$ strength associated with the α_0 decay is very small.

The extracted $E2$ component of the cross section of the ^{26}Mg$(e,e'\alpha_0)^{22}$Ne reaction is shown in Fig. 12. The same

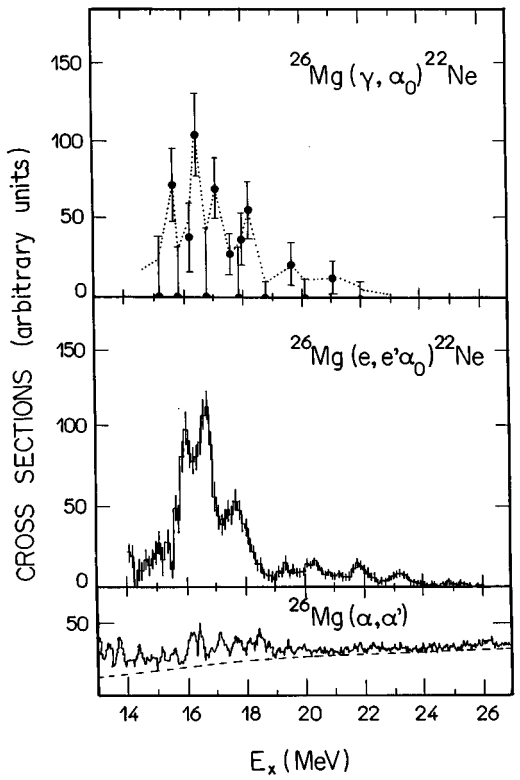

FIG. 12. $E2$ component of the cross section, obtained from the following reactions: photodisintegration [upper part, data extracted from the inverse reaction ^{22}Ne$(\alpha,\gamma_0)^{26}$Mg [9]], electrodisintegration [middle part, this work, data obtained from the ^{26}Mg$(e,e'\alpha_0)^{22}$Ne reaction for $q=0.35$ fm^{-1}], and inelastic α scattering [lower part, data from ^{26}Mg(α,α') [12]].

figure also shows the $E2$ component of ^{26}Mg$(\gamma,\alpha_0)^{22}$Ne, obtained from the inverse reaction [9] and data from ^{26}Mg(α,α') reaction [12]. Both $(e,e'\alpha_0)$ and (γ,α_0) cross sections present a bump around 16–18 MeV that shows some structure. The data from (α,α') reaction show a much richer structure, indicating that other channels besides α_0 are important in the decay process. According to the systematics of (e,e') experimental data for medium and heavy nuclei [6,43], the giant quadrupole isoscalar resonance (GQR) should be at $63A^{-1/3}$ MeV of excitation energy. For ^{26}Mg that means 22 MeV, where the $E2$ cross section of the ^{26}Mg$(e,e'\alpha_0)^{22}$Ne reaction (see Fig. 12) is very small. Thus the fraction of $E2$ excitation that decays through the α_0 channel is concentrated significantly below the expected center of the GQR. Results from (α,α') [12] indicate that this is also true for the absorption process, but with a strong fragmentation of the $E2$ strength into many different states or clusters of states. The $E2$ strength was evaluated in the same way as the $E1$. The results are shown in Table III. Although the $E2$ strength present in the α_0 channel exhausts a small fraction of the corresponding sum rule, it is about 3 times larger than the corresponding one for $E1$.

Even though the extracted $E0$ component (see lower part of Fig. 9) is spread along the whole interval of measurement, its strength is concentrated around 14–18 MeV. The relative $E0$ contribution to the total cross section is about 10 times smaller than the $E1$. Large experimental uncertainties do not allow one to draw any conclusion about its spectral characteristics. The evaluated $E0$ strength is shown in Table III, where it can be seen that the α_0 channel takes a very small fraction of the total resonance strength.

VI. CONCLUSIONS

High precision coincidence measurements of the fivefold differential cross section of the reaction ^{26}Mg$(e,e'\alpha_0)$ allowed us to obtain angular correlation functions for the emitted alphas and perform a model-independent extraction of the $E0$, $E1$, and $E2$ multipole components of this cross section.

Extracted spectra (at $q=0.35$ and 0.54 fm^{-1}) for the $E1$ component show resonance character, with a bump at 16.5 MeV, split in two peaks. The energy position of the bump is associated with the $T_<$ isospin component of the GDR. The evaluated $E1$ strength present on the α_0 channel is very small [0.45(7)% of the $E1$ EWSR].

The extracted $E2$ component of the cross section presents a bump with a fine structure (three peaks) around 16–18 MeV. The structure of the $E2$ cross section for the reaction ^{26}Mg$(e,e'\alpha_0)^{22}$Ne is similar to the one obtained from the inverse of the (γ,α_0) reaction. This structure, even though associated with the GQR, does not agree with the systematics for medium and heavy nuclei, since it is concentrated 5.5 MeV below the peak of the GQR. That is probably related to the fact [11,12] that the GQR in ^{26}Mg is fragmented into many different states, or clusters of states, spread over a large energy range, and only a very small part of it manifests itself through the α_0 channel. The $E2$ strength associated with the α_0 decay is about 3 times larger than the $E1$, but still exhausts a small fraction [1.4(3)%] of the $E2$ EWSR.

The extracted $E0$ component fluctuates over the whole measurement interval (14–26 MeV), with a slight concentration at the beginning of this interval (14–18 MeV). Only 0.2(1)% of the total $E0$ strength is associated with the α_0 decay.

The decay through the α_0 channel of the three cross sections studied ($E0$, $E1$, and $E2$ multipolarities) exhausts a small fraction of the total respective strength. This conclusion agrees with data from the inverse reaction, i.e., (α,γ_0) reaction, for $E1$ and $E2$ (there are no results for $E0$).

ACKNOWLEDGMENTS

This work has been supported in part by Fundação de Amparo à Pesquisa do Estado de São Paulo (FAPESP), Conselho Nacional de Desenvolvimento Científico e Tecnológico (CNPq), and the Deutsche Forschungsgemeinschaft (Grant No. SFB 201). One of us (L.A.A.T.) gratefully acknowledges support from the Internationales Büro, KFA, Jülich.

[1] D. DeAngelis, J. R. Calarco, J. E. Wise, H. J. Emrich, R. Neuhausen, and H. Weyand, Phys. Rev. Lett. **70**, 2872 (1993).
[2] J. P. Fritsch, H. J. Emrich, A. Grasmück, R. Neuhausen, S. Schardt, N. Zimmermann, J. R. Calarco, and M. Potokar, Phys. Rev. Lett. **68**, 1667 (1992).
[3] C. N. Papanicolas, S. E. Williamson, H. Rothhaas, G. O. Bolme, L. J. Koester, Jr., B. L. Miller, R. A. Miskimen, P. E. Mueller, and L. S. Cardman, Phys. Rev. Lett. **54**, 26 (1985).
[4] D. H. Dowell, L. S. Cardman, P. Axel, G. Bolme, and S. E. Williamson, Phys. Rev. Lett. **49**, 113 (1982).
[5] V. F. Dmitriev, D. M. Nikolenko, S. G. Popov, I. A. Rachek, D. K. Toporkov, E. P. Tsentalovich, B. B. Woitsekhowski, and V. G. Zelevinsky, Nucl. Phys. **A464**, 237 (1987).
[6] R. Pitthan and Th. Walcher, Phys. Lett. **36B**, 563 (1971).
[7] A. Hotta, K. Itoh, and T. Saito, Phys. Rev. Lett. **33**, 790 (1974).
[8] S. S. Hanna, H. F. Glavish, R. Avida, J. R. Calarco, E. Kuhlmann, and R. LaCanna, Phys. Rev. Lett. **32**, 114 (1974).
[9] E. Kuhlmann, E. Ventura, J. R. Calarco, D. G. Mavis, and S. S. Hanna, Phys. Rev. C **11**, 1525 (1975).
[10] K. T. Knöpfle, G. J. Wagner, P. Paul, H. Breuer, C. Mayer-Böricke, M. Rogge, and P. Turek, Phys. Lett. **74B**, 191 (1978).
[11] F. E. Bertrand, K. van der Borg, A. G. Drentje, M. N. Harakeh, J. van der Plicht, and A. van der Woude, Phys. Rev. Lett. **40**, 635 (1978).
[12] K. van der Borg, M. N. Harakeh, and A. van der Woude, Nucl. Phys. **A365**, 243 (1981).
[13] H. Herminghaus, A. Feder, K. H. Kaiser, W. Manz, and H. Schmitt, Nucl. Instrum. **138**, 1 (1976).
[14] H. Ehrenberg, H. Averdung, B. Dreher, G. Fricke, H. Herminghaus, and R. Neuhausen, Nucl. Instrum. **105**, 273 (1972).
[15] N. Vögler and J. Friedrich, Annual Report 1984/85, p. 146,

Institut für Kernphysik der Johannes Gutenberg Universität, Mainz, 1986.
[16] G. Herbert, Diplomarbeit, Institut für Kernphysik der Johannes Gutenberg Universität, Mainz, 1986.
[17] H. G. Andresen, H. Peter, M. Muller, H. J. Ohlbach, and P. Weber, Computer code HADES, Institut für Kernphysik der Johannes Gutenberg Universität, Mainz, 1986.
[18] C. W. de Jager, H. de Vries, and C. de Vries, At. Data Nucl. Data Tables **14**, 479 (1974).
[19] H. Überall, *Electron Scattering from Complex Nuclei* (Academic, New York, 1971), pt. B.
[20] L. C. Maximon, Rev. Mod. Phys. **41**, 193 (1969).
[21] W. E. Klepinger and J. D. Walecka, Ann. Phys. (N.Y.) **146**, 349 (1983).
[22] D. Drechsel and M. M. Giannini, Rep. Prog. Phys. **52**, 1083 (1989).
[23] L. J. Tassie, Aust. J. Phys. **9**, 407 (1956).
[24] M. Gell-Mann and V. L. Telegdi, Phys. Rev. **91**, 169 (1953).
[25] A. Bohr and B. R. Mottelson, *Nuclear Structure* (Benjamin Reading, MA, 1975), Vol. II.
[26] R. Pitthan, F. R. Buskirk, W. A. Houk, and R. W. Moore, Phys. Rev. C **21**, 28 (1980).
[27] M. Spahn, Th. Kihm, and K. T. Knöpfle, Z. Phys. A **330**, 345 (1988).
[28] O. Titze, A. Goldmann, and E. Spamer, Phys. Lett. **31B**, 565 (1970).
[29] A. Goldmann, Z. Phys. **234**, 144 (1970).
[30] S. C. Fultz, R. A. Alvarez, B. L. Berman, M. A. Kelly, D. R. Lasher, T. W. Phillips, and J. C. McElhinney, Phys. Rev. C **4**, 149 (1971).
[31] S. Fallieros, B. Goulard, and R. H. Venter, Phys. Lett. **19**, 398 (1965).
[32] E. C. Halbert, J. B. McGrory, G. R. Satchler, and J. Speth, Nucl. Phys. **A245**, 189 (1975).
[33] E. Spamer, Z. Phys. **191**, 24 (1966).
[34] T. deForest, Jr. and J. D. Walecka, Adv. Phys. **15**, 1 (1966).
[35] M. Rosen, R. Raphael, and H. Überall, Phys. Rev. **163**, 927 (1967).
[36] T. H. Schucan, Phys. Rev. **171**, 1142 (1968).
[37] M. Goldhaber and E. Teller, Phys. Rev. **74**, 1046 (1948).
[38] G. R. Satchler, Nucl. Phys. **A195**, 1 (1972).
[39] W. D. Myers, W. J. Swiatecki, T. Kodama, L. J. El-Jaick, and E. R. Hilf, Phys. Rev. C **15**, 2032 (1977).
[40] F. H. Lewis, Jr. and J. D. Walecka, Phys. Rev. **133**, 849 (1964).
[41] Th. Kihm, K. T. Knöpfle, H. Riedesel, P. Voruganti, H. J. Emrich, G. Fricke, R. Neuhausen, and R. K. M. Schneider, Phys. Rev. Lett. **56**, 2789 (1986).
[42] V. P. Likhachev, N. G. Afanas'ev, A. A. Nemashkalo, G. A. Savitskij, V. M. Khrastunov, L. D. Yaroshevskij, L. G. Lishenko, and A. T. Ushanev, Sov. J. Nucl. Phys. **23**, 261 (1976).
[43] S. Fukuda and Y. Torizuka, Phys. Rev. Lett. **29**, 1109 (1972).